Zhao, X. and Chen, Q. 2019. "Inverse design of indoor environment using an adjoint RNG k-ε turbulence model," *Indoor Air*, 29: 320-330.

Inverse design of indoor environment using an adjoint RNG k-ε turbulence model

X. Zhao[1] and Q. Chen [2,*]

[1]Tianjin Key Laboratory of Indoor Air Environmental Quality Control, School of Environmental Science and Engineering, Tianjin University, Tianjin 300072, China
[2]School of Mechanical Engineering, Purdue University, West Lafayette, IN 47907, USA

Corresponding author's phone: (765) 496-7562, email address: yanchen@purdue.edu

Abstract

The adjoint method can determine design variables of an indoor environment according to the optimal design objective, such as minimal predicted mean vote (PMV) for thermal comfort. The method calculates the gradient of the objective function over the design variables so that the objective function can be minimized along the fastest direction using an optimization algorithm. Since the objective function is controlled by the Reynolds-averaged Navier-Stokes (RANS) equations with the RNG k-ε model during the optimization process, all the corresponding adjoint equations should be solved, rather than the "frozen turbulence" assumption used in previous studies. This investigation developed adjoint equations for the RNG k-ε turbulence model and applied it to a two-dimensional ventilated cavity and a three-dimensional, two-person office. Design processes with the adjoint RNG k-ε turbulence model led to a near-zero design function for the two cases, while those with the "frozen turbulence" assumption did not. This investigation has successfully used the new method to design a two-person office with optimal thermal comfort level around the two occupants.

KEYWORDS

Inverse design, Indoor environment, Adjoint method, Numerical algorithm, Validation, Turbulence model

Practical Implications

This investigation developed an adjoint RNG k-ε turbulence model for optimal design of the indoor environment. The adjoint method with the adjoint RNG k-ε turbulence model can be used to design the optimal indoor environment for buildings. Design objective could include air velocity distribution, temperature distribution, and the combination of variables calculated by CFD, such as thermal comfort, indoor air quality, etc.

Nomenclature

g	gravity vector
J	objective function
k	turbulent kinetic energy
k_a	adjoint turbulent kinetic energy
L	augmented objective function
N	incompressible Navier-Stokes equations in vector form

p	air pressure
p_a	adjoint pressure
R	residual form of the RNG k-ε turbulence model equations
T	air temperature
T_a	adjoint temperature
T_{op}	operating air temperature
V	air velocity
$\mathbf{V_a}$	adjoint velocity

Subscripts

a	adjoint method
op	operate

Greek symbols

γ	thermal expansion coefficient of air
δ	small constant set by a designer
ε	turbulent energy dissipation rate
ε_a	adjoint turbulent energy dissipation rate
Θ	design domain
κ	effective thermal conductivity
ν	kinematic (laminar) viscosity
ν_{eff}	effective viscosity
ν_k	effective diffusivity for k
ν_t	turbulent viscosity
ν_ε	effective diffusivity for ε
ξ	design variables

1 INTRODUCTION

To create a thermally comfortable and healthy indoor environment, conventional designs use a trial-and-error process[1] that assumes certain thermo-fluid boundary conditions (B.C.), such as air supply inlet size, number, and locations, air supply velocity and temperature, etc. An appropriate method is then used to estimate the resulting distributions of air temperature, velocity, relative humidity, and contaminant concentrations. The trial-and-error process is very time consuming because the assumed thermo-fluid B.C. may not be desirable. Recently, inverse or optimal design processes[2] have emerged, such as the computational fluid dynamics (CFD)-based[3] genetic algorithm (GA) method[4], CFD-based proper orthogonal decomposition (POD) method[5], CFD-based artificial neural network (ANN) method[6], and adjoint method[7].

To design a desirable indoor environment, the CFD-based GA method must calculate a large number of samples, and the number of calculations increases exponentially with the number of design variables. To reduce computing effort, Wei et al.[5] developed a CFD-based POD method that can transform the nonlinear problem into a linear one and build a cause-effect mapping relationship between the objective function and design variables. Since it is a reduced-order method, the accuracy of this method is greatly reduced. The CFD-based ANN

method can also build the mapping relationship between the objective function and design variables, in this case by selecting a certain number of samples to train the ANN model. With a well-trained ANN model, the design objective can be predicted without CFD calculations. However, the accuracy of this method depends on the number of samples. In addition, the mapping relationship established by either the CFD-based POD method or the CFD-based ANN method is applicable only to a specific case. For a different case, the relationship would change. The adjoint method can quickly find the optimal design of an indoor environment using an optimization algorithm without building a mapping relationship for each new problem, although it may become trapped in local optima[8]. The adjoint method is the most efficient and suitable method for the inverse design of a thermally comfortable and healthy indoor environment.

The adjoint method was developed recently[9] for inversely designing an indoor environment by solving a set of Navier-Stokes equations and adjoint equations, alternatively. The adjoint equations are derived from the continuous Navier-Stokes equations[10]. Liu and Chen[9] used the adjoint method to inversely identify the thermo-fluid B.C. required to achieve the optimal design of ventilation for an enclosed environment. Liu et al.[11] then adopted this method to improve the thermal comfort level for an airline cabin. Zhao et al.[12] also attempted to use the adjoint method combined with area-constrained topology and cluster analysis to design a thermally comfortable indoor environment. However, the results of these studies indicated that this method cannot make the objective functions reach the ideal values. One reason may be that the objective functions become trapped in local optima. Another reason may be that the adjoint method, which was used in previous studies[9, 11-14], derives only the adjoint equations of the RANS equations with the "frozen turbulence" assumption. With the assumption, the k and ε will not feel changes of the design variables and use the solution (k and ε) of the flow equations when the adjoint equations are solved. The assumption can reduce deriving manually effort[14, 15] by neglecting variations in the turbulent variables. However, this method can provide only approximate gradients, or even incorrect gradients, which may not lead to global optima for the design.

A variant of the method is the discrete adjoint method[16], which first discretizes the Navier-Stokes equations and then derives the discrete adjoint equations from the discrete Navier-Stokes equations. Since the discrete adjoint method derives the complete adjoint equations that include the adjoint equations for calculating turbulent viscosity, it can provide accurate gradients[17]. However, it requires a large amount of computational memory, which may not be affordable in practice. To obtain accurate gradients and reduce computational memory, one option is to develop a continuous adjoint method without using the "frozen turbulence" assumption[18].

Since the turbulent viscosity ν_t in the momentum equation can be solved by introducing an appropriate turbulence model, some studies have derived the complete continuous adjoint equations with an appropriate adjoint turbulence model. Zymaris et al. proposed a Spalart-Allmaras one-equation adjoint turbulence model[19] and a standard k-ε adjoint turbulence model[20] to minimize duct pressure losses. Papoutsis-Kiachagias[21] developed a

low-Reynolds-number Launder-Sharma k-ε adjoint turbulence model to optimize duct shape, with the aim of minimizing viscous losses. All these applications have proved that an appropriate adjoint turbulence model can provide an accurate gradient of the objective function over the design variables. However, none of the above turbulence models is suitable for inversely designing an indoor environment. Chen[22], Conceição et al.[23], Zhang et al.[24] and Zhang et al.[25] compared different turbulence models and found that the RNG k-ε turbulence model shows the best overall performance for solving indoor airflow among various RANS models. In addition, there do not have the corresponding adjoint equation. Therefore, this study aimed to develop an adjoint RNG k-ε turbulence model for inversely designing an indoor environment.

2 METHODS

2.1 Adjoint method with adjoint RNG k-ε turbulence model

To design an indoor environment using the adjoint method, we must first construct a suitable objective function. For example, the objective function J is a desirable distribution of air velocity **V** and temperature T in the design domain Θ:

$$\mathrm{J}(\boldsymbol{\xi}) = \int_{\Theta} f(\mathbf{V}, T)\mathrm{d}\Theta \tag{1}$$

where $\boldsymbol{\xi}$ is a vector that represents the design variables, such as air supply inlet size, number, and locations; air supply velocity, $\mathbf{V}_{\mathrm{inlet}}$; air supply temperature, $\mathrm{T}_{\mathrm{inlet}}$, etc., that could lead to the desirable distribution. In this study, air velocity **V** and temperature T in the design domain Θ, as shown in Eq. (1), are controlled by the incompressible, steady-state RANS equations, as shown in Eqs. (2), (3), and (4), closed with the RNG k-ε turbulence model[26], as expressed by Eqs. (5) and (6).

$$\mathrm{N}_1 = -\nabla\cdot\mathbf{V} = 0 \tag{2}$$

$$(\mathrm{N}_2, \mathrm{N}_3, \mathrm{N}_4)^{\mathrm{T}} = (\mathbf{V}\cdot\nabla)\mathbf{V} + \nabla\mathrm{p} - \nabla\cdot(2\nu_{eff}\mathrm{D}(\mathbf{V})) - \gamma\mathbf{g}(\mathrm{T}-\mathrm{T}_{\mathrm{op}}) = 0 \tag{3}$$

$$\mathrm{N}_5 = \nabla\cdot(\mathbf{V}\mathrm{T}) - \nabla\cdot(\kappa\nabla\mathrm{T}) = 0 \tag{4}$$

$$\mathrm{R}_1 = \nabla\cdot(\mathbf{V}\mathrm{k}) - \nabla\cdot(\nu_{\mathrm{k}}\nabla\mathrm{k}) - \nu_{\mathrm{t}}\mathrm{P}_{\mathrm{k}} - \mathrm{G}_{\mathrm{b}} + \varepsilon = 0 \tag{5}$$

$$\begin{aligned}\mathrm{R}_2 = {} & \nabla\cdot(\mathbf{V}\varepsilon) - \nabla\cdot(\nu_{\varepsilon}\nabla\varepsilon) - \left[\mathrm{C}_{\varepsilon 1}(\nu_{\mathrm{t}}\mathrm{P}_{\mathrm{k}} + \mathrm{C}_{\varepsilon 3}\mathrm{G}_{\mathrm{b}}) - \mathrm{C}_{\varepsilon 2}\varepsilon\right]\frac{\varepsilon}{\mathrm{k}} \\ & + \frac{\mathrm{C}_{\mu}\eta^3(1-\eta/\eta_0)}{1+\beta\eta^3}\frac{\varepsilon^2}{\mathrm{k}} = 0\end{aligned} \tag{6}$$

where

$$\nu_{eff} = \nu + \nu_t;\ \nu_t = c_\mu \frac{k^2}{\varepsilon};\ P_k = \left(\frac{\partial V_i}{\partial x_j} + \frac{\partial V_j}{\partial x_i}\right)\frac{\partial V_i}{\partial x_j};\ i, j = x, y, z;$$
$$\eta = Sk/\varepsilon;\ S = \sqrt{(2S_{ij}S_{ij})};\ S_{ij} = \frac{1}{2}\left(\frac{\partial V_i}{\partial x_j} + \frac{\partial V_j}{\partial x_i}\right);\ G_b = \frac{\nu_t}{Pr_t}\gamma \mathbf{g}\nabla T \quad (7)$$

In these equations, p represents the air pressure; $D(\mathbf{V}) = (\nabla\mathbf{V}+(\nabla\mathbf{V})^T)/2$ is the rate of strain tensor; k is the turbulent kinetic energy; ε is the turbulent energy dissipation; $c_\mu = 0.0845$; $\eta_0 = 4.38$; $\beta = 0.012$; $C_{\varepsilon 1} = 1.42$; $C_{\varepsilon 2} = 1.68$; $C_{\varepsilon 3} = 1$; G_b is the buoyancy production rates of turbulent kinetic energy; P_k is the shear production rates of the turbulence kinetic energy; Pr_t turbulence Prandtl number for temperature; S is the modulus of the mean rate-of-strain tensor; **N** represents the incompressible, steady-state RANS equations in residual form; and **R** represents the residual form of the RNG k-ε turbulence model equations.

To minimize the objective function as shown in Eq. (1), this investigation used the steepest decent method[27] as shown in Eq. (8) to update the design variables. Therefore, the adjoint method was used to calculate the gradients used in Eq. (8).

$$\xi_{n+1} = \xi_n - \lambda_n \frac{dJ}{d\xi_n} \quad (8)$$

where ξ_n, ξ_{n+1} are design variables at current and succeeding design cycles, respectively; n represents the design cycle and λ is the constant step size.

The adjoint method introduces an augmented objective function L as shown in Eq. (9) and transforms the constrained design problem into an unconstrained optimization problem.

$$L = J + \int_\Omega \left(p_a, \mathbf{V_a}, T_a, k_a, \varepsilon_a\right)\cdot\left(\mathbf{N}, \mathbf{R}\right) d\Omega \quad (9)$$

where Ω represents the computational domain and p_a, $\mathbf{V}_a$, T_a, k_a, and ε_a are the adjoint pressure, adjoint velocity, adjoint temperature, adjoint turbulence kinetic energy, and adjoint rate of dissipation of turbulent energy, respectively.

From Eq. (9) we can then derive the following adjoint equations of the RANS equations closed with the RNG k-ε turbulence model. Detailed intermediate derivation process of the adjoint equations can be found in[12].

- Adjoint continuity equation:

$$-\nabla\cdot\mathbf{V_a} + \frac{\partial J_\Omega}{\partial p} = 0 \quad (10)$$

- Adjoint momentum equation:

$$
\begin{aligned}
&-\nabla\mathbf{V_a}\cdot\mathbf{V}-(\mathbf{V}\cdot\nabla)\mathbf{V_a}+\nabla \mathrm{p_a}-\nabla\cdot\left(2\nu_{eff}\mathrm{D}(\mathbf{V_a})\right)-\mathrm{T}\nabla\mathrm{T_a}-\mathrm{k}\nabla\mathrm{k_a}\\
&-\varepsilon\nabla\varepsilon_{\mathrm{a}}+2\frac{\partial}{\partial \mathrm{x_j}}\left[\left(\mathrm{k_a}+\varepsilon_{\mathrm{a}}\mathrm{C}_{\varepsilon 1}\frac{\varepsilon}{\mathrm{k}}\right)\nu_{\mathrm{t}}\left(\frac{\partial \mathrm{V_i}}{\partial \mathrm{x_j}}+\frac{\partial \mathrm{V_j}}{\partial \mathrm{x_i}}\right)\right]+\frac{\partial \mathrm{J}_{\Omega}}{\partial \mathbf{V}}\\
&-\frac{\partial}{\partial \mathrm{x_j}}\left[\varepsilon_{\mathrm{a}}\left(\frac{3\eta^2-4\eta^3/\eta_0}{1+\beta\eta^3}-\frac{\left(\eta^3-\eta^4/\eta_0\right)3\beta\eta^2}{\left(1+\beta\eta^3\right)^2}\right)\mathrm{C}_{\mu}\varepsilon\right]=0
\end{aligned}
\tag{11}
$$

- Adjoint energy equation:

$$
\begin{aligned}
&-(\mathbf{V}\cdot\nabla)\mathrm{T_a}-\nabla\cdot\left(\kappa\nabla\mathrm{T_a}\right)-\gamma\left(\mathbf{V_a}\cdot\mathbf{g}\right)+\frac{\nu_{\mathrm{t}}}{\mathrm{Pr_t}}\gamma\mathbf{g}\nabla\mathrm{k_a}\\
&+\mathrm{C}_{\varepsilon 1}\mathrm{C}_{\varepsilon 3}\frac{\nu_{\mathrm{t}}}{\mathrm{Pr_t}}\frac{\varepsilon}{\mathrm{k}}\gamma\mathbf{g}\nabla\varepsilon_{\mathrm{a}}+\frac{\partial \mathrm{J}_{\Omega}}{\partial \mathrm{T}}=0
\end{aligned}
\tag{12}
$$

- Adjoint turbulent kinetic energy equation:

$$
\begin{aligned}
&-\mathbf{V}\nabla k_a-\nabla\cdot\left(\nu_k\nabla k_a\right)+4\nu_t\frac{1}{k}D(\mathbf{V})\nabla\mathbf{V_a}+\frac{2\nu_t}{Pr_t}\frac{1}{k}\nabla T\nabla T_a+\frac{2\nu_t}{\sigma_k}\frac{1}{k}\nabla k\nabla k_a\\
&+\frac{2\nu_t}{\sigma_k}\frac{1}{k}\nabla\varepsilon\nabla\varepsilon_a-2\nu_t k_a\frac{1}{k}P_k-k_a\frac{2\nu_t}{Pr_t}\frac{1}{k}\gamma\mathbf{g}\nabla T-\varepsilon_a C_{\varepsilon 1}\nu_t P_k\frac{\varepsilon}{k^2}\\
&-\varepsilon_a C_{\varepsilon 1}C_{\varepsilon 3}\frac{\nu_t}{Pr_t}\gamma\mathbf{g}\nabla T\frac{\varepsilon}{k^2}-\varepsilon_a C_{\varepsilon 2}\frac{\varepsilon^2}{k^2}+\frac{\partial J_{\Omega}}{\partial k}\\
&+\varepsilon_a\left[\left(\frac{3\eta^2-4\eta^3/\eta_0}{1+\beta\eta^3}-\frac{\left(\eta^3-\eta^4/\eta_0\right)3\beta\eta^2}{\left(1+\beta\eta^3\right)^2}\right)C_{\mu}\frac{\eta\varepsilon^2}{k^2}-\frac{C_{\mu}\eta^3\left(1-\eta/\eta_0\right)}{1+\beta\eta^3}\frac{\varepsilon^2}{k^2}\right]=0
\end{aligned}
\tag{13}
$$

- Adjoint equation for the dissipation rate of turbulent kinetic energy:

$$
\begin{aligned}
&-\mathbf{V}\nabla\varepsilon_a-\nabla\cdot\left(\nu_\varepsilon\nabla\varepsilon_a\right)-2\nu_t\frac{1}{\varepsilon}D(\mathbf{V})\nabla\mathbf{V_a}-\frac{\nu_t}{Pr_t}\frac{1}{\varepsilon}\nabla T\nabla T_a-\frac{\nu_t}{\sigma_k}\frac{1}{\varepsilon}\nabla k\nabla k_a-\frac{\nu_t}{\sigma_\varepsilon}\frac{1}{\varepsilon}\nabla\varepsilon\nabla\varepsilon_a\\
&+k_a\nu_t\frac{1}{\varepsilon}P_k+k_a\frac{\nu_t}{Pr_t}\frac{1}{\varepsilon}\gamma\mathbf{g}\nabla T+k_a+2\varepsilon_a C_{\varepsilon 2}\frac{\varepsilon}{k}+\frac{\partial J_{\Omega}}{\partial\varepsilon}\\
&+\varepsilon_a\left[-\left(\frac{3\eta^2-4\eta^3/\eta_0}{1+\beta\eta^3}-\frac{\left(\eta^3-\eta^4/\eta_0\right)3\beta\eta^2}{\left(1+\beta\eta^3\right)^2}\right)C_{\mu}\frac{\eta\varepsilon}{k}+\frac{C_{\mu}\eta^3\left(1-\eta/\eta_0\right)}{1+\beta\eta^3}\frac{2\varepsilon}{k}\right]=0
\end{aligned}
\tag{14}
$$

We also give final gradient of the augmented objective function over the design variables:

$$\frac{\mathrm{dL}}{\mathrm{dV}_{\mathrm{inlet,i}}}=\left(\begin{array}{l}\mathbf{S}_{\mathrm{inlet}}\mathrm{p}_{\mathrm{a,inlet}}+\left(\mathbf{S}_{\mathrm{inlet}}\cdot\mathbf{V}_{\mathrm{inlet}}\right)\mathbf{V}_{\mathrm{a,inlet}}+\mathbf{S}_{\mathrm{inlet}}\left(\mathbf{V}_{\mathrm{inlet}}\cdot\mathbf{V}_{\mathbf{a},\mathrm{inlet}}\right)-\dfrac{\nu_{eff}\left|\mathbf{S}_{\mathrm{inlet}}\right|}{\left|\mathbf{d}_{\mathrm{n}}\right|}\mathbf{V}_{\mathrm{a,inlet}}\\ +\mathbf{S}_{\mathrm{inlet}}\mathrm{T}_{\mathrm{inlet}}\mathrm{T}_{\mathrm{a,inlet}}+\mathbf{S}_{\mathrm{inlet}}\mathrm{k}_{\mathrm{inlet}}\mathrm{k}_{\mathrm{a,inlet}}+\mathbf{S}_{\mathrm{inlet}}\varepsilon_{\mathrm{inlet}}\varepsilon_{\mathrm{a,inlet}}\end{array}\right)\cdot\mathbf{e}_{\mathrm{i}} \tag{15}$$

$$\begin{aligned}\frac{\mathrm{dL}}{\mathrm{dT}_{\mathrm{inlet}}}=&-\gamma\mathbf{g}\cdot\mathbf{V}_{\mathrm{a,inlet}}\mathrm{Vol}_{\mathrm{inlet}}+\mathbf{S}_{\mathrm{inlet}}\cdot(\mathbf{V}_{\mathrm{inlet}}\mathrm{T}_{\mathrm{a,inlet}}-\kappa\frac{\mathbf{d}_{\mathrm{n}}}{\left|\mathbf{d}_{\mathrm{n}}\right|\left|\mathbf{d}_{\mathrm{n}}\right|}\mathrm{T}_{\mathrm{a,inlet}}+\frac{\nu_{\mathrm{t}}}{\mathrm{Pr}_{\mathrm{t}}}\gamma\mathbf{g}\mathrm{k}_{\mathrm{a,inlet}}\\ &+\mathrm{C}_{\varepsilon1}\mathrm{C}_{\varepsilon3}\frac{\nu_{\mathrm{t}}}{\mathrm{Pr}_{\mathrm{t}}}\frac{\varepsilon}{\mathrm{k}}\gamma\mathbf{g}\varepsilon_{\mathrm{a,inlet}})\end{aligned} \tag{16}$$

where $\mathrm{V}_{\mathrm{inlet,\,i}}$ is the inlet air velocity in the i^{th} direction, i = x, y, z; $\mathbf{S}_{\mathrm{inlet}}$ is the outward-pointing face area vector of inlet cell; $\mathrm{p}_{\mathrm{a,\,inlet}}$, $\mathbf{V}_{\mathrm{a,\,inlet}}$, $\mathrm{T}_{\mathrm{a,\,inlet}}$, $\mathrm{k}_{\mathrm{a,\,inlet}}$ and $\varepsilon_{\mathrm{a,\,inlet}}$ are the adjoint pressure, adjoint velocity, adjoint temperature, the adjoint turbulent kinetic energy and the adjoint turbulent energy dissipation rate at the cell adjacent to the corresponding boundary face, respectively; $\mathrm{k}_{\mathrm{inlet}}$ and $\varepsilon_{\mathrm{inlet}}$ are the turbulent kinetic energy and the turbulent energy dissipation rate at inlet boundary face, respectively; $\mathbf{d}_{\mathrm{n}}$ is the direction vector between an inlet cell center and the boundary face center; $\mathbf{e}_{\mathrm{i}}$ is the unit vector in the i^{th} direction, i = x, y, z; $\mathrm{Vol}_{\mathrm{inlet}}$ is the inlet cell volume. When the RANS equations closed with the RNG k-ε turbulence model and the adjoint equations are numerically solved in succession, all state fields and adjoint fields needed for calculating the gradient of the objective function over the design variables are available.

2.2 Adjoint boundary conditions

The adjoint inlet boundary conditions are that zero p_{a}, $\mathbf{V}_{\mathrm{a}}$, T_{a}, k_{a}, and ε_{a} along the inlet. $\mathbf{V}_{\mathrm{a}}$, T_{a}, k_{a}, and ε_{a} are set to zero and zero gradient boundary condition of p_{a} at the wall. While the adjoint outlet boundary conditions can be determined by:

$$\begin{aligned}&\boldsymbol{n}\left(\mathbf{V}_{\mathbf{a}}\cdot\mathbf{V}\right)+\mathbf{V}_{\mathbf{a}}\left(\mathbf{V}\cdot\boldsymbol{n}\right)+\nu_{eff}\left(\boldsymbol{n}\cdot\nabla\right)\mathbf{V}_{\mathbf{a}}-\mathrm{p}_{\mathrm{a}}\boldsymbol{n}+\mathrm{T}_{\mathrm{a}}\boldsymbol{n}\mathrm{T}+\mathrm{k}_{\mathrm{a}}\boldsymbol{n}\mathrm{k}+\varepsilon_{\mathrm{a}}\boldsymbol{n}\varepsilon\\ &-2\left(\mathrm{k}_{\mathrm{a}}+\varepsilon_{\mathrm{a}}\mathrm{C}_{\varepsilon1}\frac{\varepsilon}{\mathrm{k}}\right)\nu_{\mathrm{t}}\left(\frac{\partial\mathrm{V}_{\mathrm{i}}}{\partial\mathrm{x}_{\mathrm{j}}}+\frac{\partial\mathrm{V}_{\mathrm{j}}}{\partial\mathrm{x}_{\mathrm{i}}}\right)\boldsymbol{n}_{j}+\frac{\partial\mathrm{J}_{\Gamma}}{\partial\mathbf{V}}\\ &+\varepsilon_{\mathrm{a}}\left(\frac{3\eta^{2}-4\eta^{3}/\eta_{0}}{1+\beta\eta^{3}}-\frac{\left(\eta^{3}-\eta^{4}/\eta_{0}\right)3\beta\eta^{2}}{\left(1+\beta\eta^{3}\right)^{2}}\right)\mathrm{C}_{\mu}\varepsilon\boldsymbol{n}_{j}=0\end{aligned} \tag{17}$$

$$\mathrm{T}_{\mathrm{a}}\boldsymbol{n}\mathbf{V}+\boldsymbol{n}\kappa\nabla\mathrm{T}_{\mathrm{a}}-\mathrm{k}_{\mathrm{a}}\frac{\nu_{\mathrm{t}}}{\mathrm{Pr}_{\mathrm{t}}}\gamma\mathbf{g}\boldsymbol{n}-\varepsilon_{\mathrm{a}}\mathrm{C}_{\varepsilon1}\mathrm{C}_{\varepsilon3}\frac{\nu_{\mathrm{t}}}{\mathrm{Pr}_{\mathrm{t}}}\frac{\varepsilon}{\mathrm{k}}\gamma\mathbf{g}\boldsymbol{n}+\frac{\partial\mathrm{J}_{\Gamma}}{\partial\mathrm{T}}=0 \tag{18}$$

$$\nu_{k}\boldsymbol{n}\nabla k_{a}+k_{a}\boldsymbol{n}\mathbf{V}-\frac{2\nu_{t}}{Pr_{t}}\frac{1}{k}\nabla T\boldsymbol{n}T_{a}-\mathbf{V}_{\mathbf{a}}4\nu_{t}\frac{1}{k}D\left(\mathbf{V}\right)\boldsymbol{n}+\frac{\partial J_{\Gamma}}{\partial k}=0 \tag{19}$$

$$2\nu_t \frac{1}{\varepsilon} D(\mathbf{V})\mathbf{V_a}\boldsymbol{n} + \varepsilon_a \mathbf{V}\boldsymbol{n} + \nu_\varepsilon \boldsymbol{n}\nabla\varepsilon_a + \frac{\partial J_\Gamma}{\partial \varepsilon} = 0 \quad (20)$$

where $\boldsymbol{n}$ is the normal component and J_Γ is the objective function defined on boundary.

2.3 Numerical method

The adjoint method with the "frozen turbulence" assumption and the adjoint RNG k-ε turbulence model were previously implemented in OpenFOAM (Open Field Operation And Manipulation) [29]. The convection and diffusion terms of the RANS equations closed with the turbulence model and adjoint equations were discretized by the first-order upwind scheme and the central difference scheme, respectively. Previous studies[1,7-9, 11-13] all used the first-order upwind scheme to discretize the convection terms of both set of equations and none of the studies have not reported any accuracy issues. Thus, we used the same scheme and did not explore high-order numerical scheme. The Boussinesq approximation[30] was used to simulate the thermal plume generated by the temperature difference. The convergence criterion was set as $|J_n - J_{n-1}| < \delta$ (where $n \geq 2$ and $\delta = 10^{-3}$), where J_{n-1}, J_n are the objective function at previous and current design cycles, respectively.

3 RESULTS

In order to verify the performance of the adjoint RNG k-ε turbulence model for inverse design of an indoor environment, this study first tested the proposed method by applying it to a two-dimensional ventilated cavity[31] and a two-person office[32] through a step-by-step process. The two-dimensional ventilated cavity is a simple case with mixed ventilation, while the three-dimensional ventilated office represents a complete indoor environment with complex geometries and displacement ventilation. To prove the accuracy of the proposed method and the necessity of developing a new method, the adjoint method with the "frozen turbulence" assumption was conducted as a comparison. Finally, this study used the validated method to inversely design an optimal indoor environment for the two-person office.

3.1 Two-dimensional ventilated cavity

The first case is a simple two-dimensional ventilated cavity, as shown in Figure 1, with experimental data (i.e., velocity and temperature) along the green center lines and detailed information about all B.C. available[31]. The experiment supplied air through the inlet at the top of the left wall and exhausted air through the outlet at the bottom of the right wall. With the exception of the floor, which was heated to 35.5 ºC, the temperatures of the ceiling and walls were all controlled at 15.0 ºC.

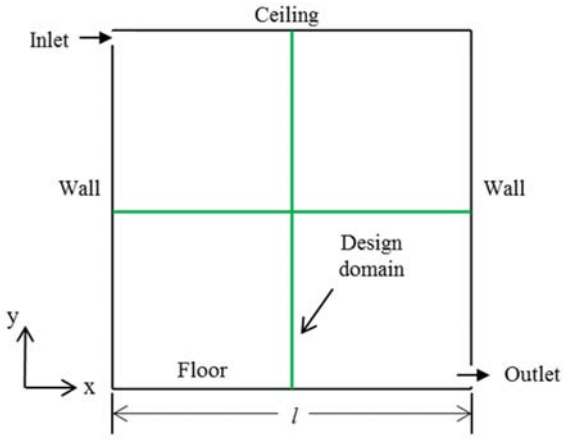

FIGURE 1 Schematic of a two-dimensional ventilated cavity

- CFD simulation:

Before starting the inverse design process, we needed to prove that we had the ability to conduct the CFD simulation correctly. This investigation conducted CFD simulation using experimental B.C. Experimental data along the green center lines was used to verify the results of the simulation. Figure 2 compares the air velocity and temperature profiles predicted by CFD with the RNG k-ε turbulence model and the experimental data at x = 0.5 *l*. The comparison indicates that we were able to predict the air distribution accurately in the ventilated cavity. However, the simulation results did not coincide completely with the experimental results. The mean relative error of the air temperature between the CFD simulation results and the experimental data is 2.2%. However, the mean relative error of the air velocity is a little higher, that is because the velocity at the center of the cavity is very small. Thus, there were errors between the experimental data and the results predicted by CFD. The discrepancies may have arisen from measurement errors and uncontrollable factors in the experiment and numerical errors in the CFD simulation, especially the RNG k-ε model. Such errors may affect the inverse design results. If the experimental data along the green lines were used as target function for inverse modeling, the solution would not be ideal due to the inherited errors from the CFD in the adjoint equations. Thus, it is better to use CFD results along the green lines as target function because the numerical errors in the CFD simulation are the same as those in the inversed simulation.

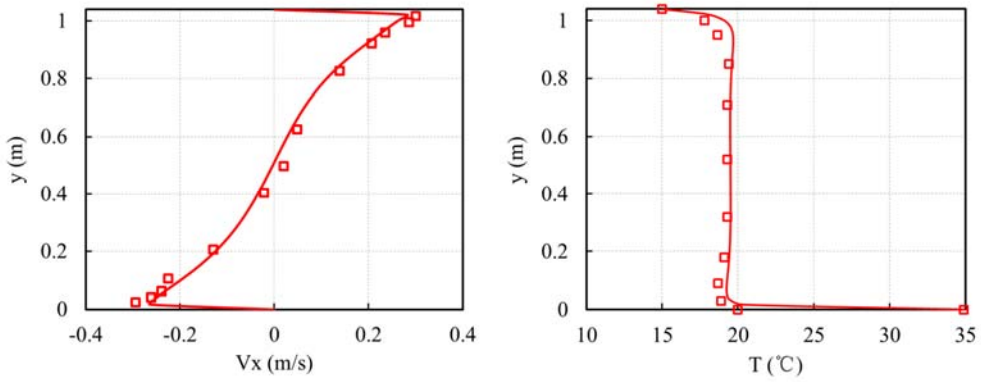

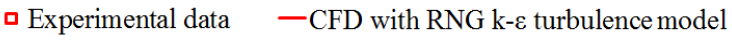

FIGURE 2 Comparison of air velocity and temperature profiles predicted by CFD with the RNG k-ε turbulence model and experimental data from Blay et al.[31] along the x = 0.5 *l* section.

- Inverse design process:

Since our purpose was to verify the performance of the proposed method using the numerical method, we set the CFD simulation results along the two mid-sections (green lines) as target values to eliminate the influence of experimental errors and numerical errors, and the air supply parameters as the design variables to construct the objective function. If the air supply parameters identified were found to be consistent with the experimental air supply parameters, the proposed method would be verified. For this case, we used the predicted air velocity $\mathbf{V}_{0,ii}$ (vector) and air temperature $T_{0,ii}$ in a design domain (the values along the two mid-sections), Θ, as the target values to construct the objective function, which can be expressed as:

$$J(\xi) = W_1 * V_{norm} \sum_{ii=1}^{m} \left| \mathbf{V}_{ii} - \mathbf{V}_{0,ii} \right|^2 + W_2 * T_{norm} \sum_{ii=1}^{m} \left(T_{ii} - T_{0,ii} \right)^2 \quad (21)$$

where

$$V_{norm} = \frac{1}{V_{inlet,x}^2}; T_{norm} = \frac{1}{\left(T_{max} - T_{min} \right)^2} \quad (22)$$

where W_1 and W_2 are the weighting factors, assumed to be 0.5 in this study; V_{norm} and T_{norm} are the normalization factors; and T_{max} and T_{min} are equal to 35.5ºC and 15.0ºC, respectively; m is the total number data in the design domain; $\mathbf{V}_{ii}$ and T_{ii} are the inversely designed results in the design domain, in this case, respectively. With the above objective function, the adjoint method with the adjoint RNG k-ε turbulence model started its inverse design process from the initial inlet B.C. These B.C. were $\mathbf{V}_{inlet}$ = (0.8, 0) m/s and T_{inlet} = 22.0ºC. For each design cycle, both the RANS equations closed with the turbulence model and the adjoint equations were calculated with the use of 2,000 iterations to ensure convergence.

To study the accuracy of the gradient calculated by the proposed method and rule out the influence of step size, we adopted the steepest descent method with proper constant step size in Eq. (8) to update the design variables. Since an improper constant step size could cause the objective function to become trapped in local optima or the calculation to diverge, this investigation test different step sizes for proper step sizes (0.016 for updating V_{inlet} is 0.016 and 200 for updating T_{inlet}).

With the proper step sizes and the same initialized air supply parameters, we also used the adjoint method with the "frozen turbulence" assumption to inversely identify the optimal design variables for the ventilated cavity, in order to illustrate the need for the new method. Figure 3 compared the k with k_a (adjoint k) of these two methods when solving the adjoint

equations at the first design cycle that was because these two methods have the same air supply parameters only in this design cycle during the inverse design process. The k is the turbulent energy, while the k_a is adjoint turbulent energy. The turbulent energy represents the degree of chaos of the flow, while the adjoint turbulent energy is the opposite. They are very different because two sets of equations are different. As a result, the gradients calculated by these two methods are different. When the objective function minimized by the adjoint method with the "frozen turbulence" assumption met the convergence criteria, as shown in Figure 4, the objective function minimized by the adjoint RNG k-ε turbulence model reached the same value at almost the same time. However, the new method can cause the objective function to continue to decrease. The design variables identified by the adjoint RNG k-ε turbulence model for Case A-2 were almost the same as the known experimental data, as shown in Table 1. This indicates that the adjoint RNG k-ε turbulence model has higher calculation accuracy.

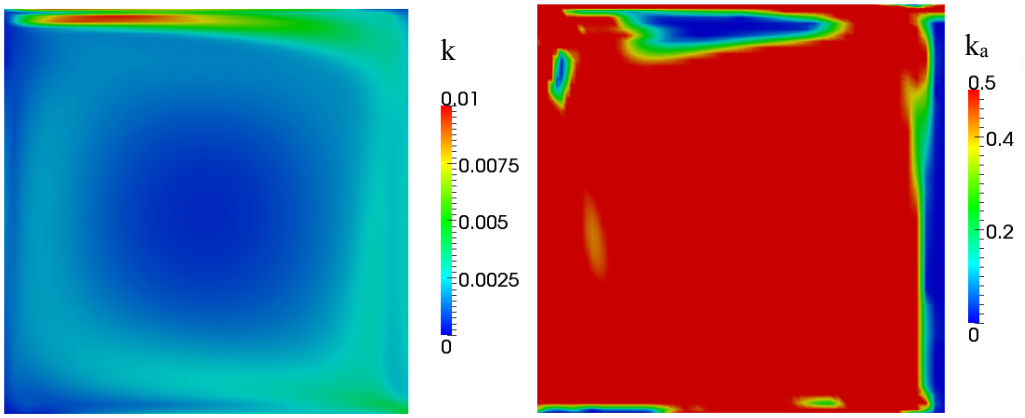

(a) (b)

FIGURE 3 Comparison of (a) k solution of the flow equation and (b) k_a calculated by the adjoint RNG k-ε turbulence model at the first design cycle

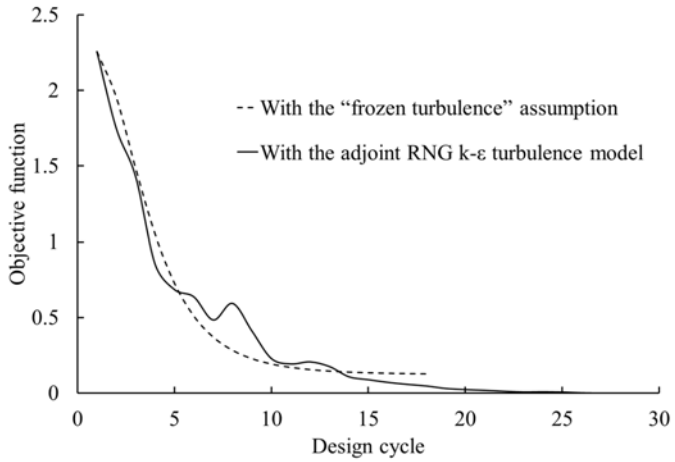

FIGURE 4 Variation in the objective function with the design cycle for the two-dimensional ventilated cavity

TABLE 1 Design variables identified by two methods compared with the experimental B.C.

	$V_{inlet, x}$ (m/s)	$V_{inlet, y}$ (m/s)	T_{inlet} (K)	J
With the "frozen turbulence" assumption	0.54	4.3E-4	287.36	0.13
With the adjoint RNG k-ε turbulence model	0.56	7.2 E-3	288.15	4.2 E-4
Experimental data[31]	0.57	0	288.15	

After the optimal air supply parameters, as shown in Table 1, had been identified by the two methods, we conducted CFD simulation with the RNG k-ε turbulence model to determine whether the optimized air distribution was consistent with the target values (red line/dots). Figure 5 illustrates the velocity vector and temperature profiles in the design domain predicted with the air supply parameters identified by the adjoint method with the "frozen turbulence" assumption (green line/dots) and with the adjoint RNG k-ε turbulence model (blue lines/dots). The air distribution in the design domain optimized with the adjoint RNG k-ε turbulence model was closer to the target values than the distribution optimized with the "frozen turbulence" assumption, especially in the center of the design domain. The air temperatures at x = 0.5 *l* predicted with the "frozen turbulence" assumption were also much lower than the actual values. Thus, the performance of the adjoint RNG k-ε turbulence model was better.

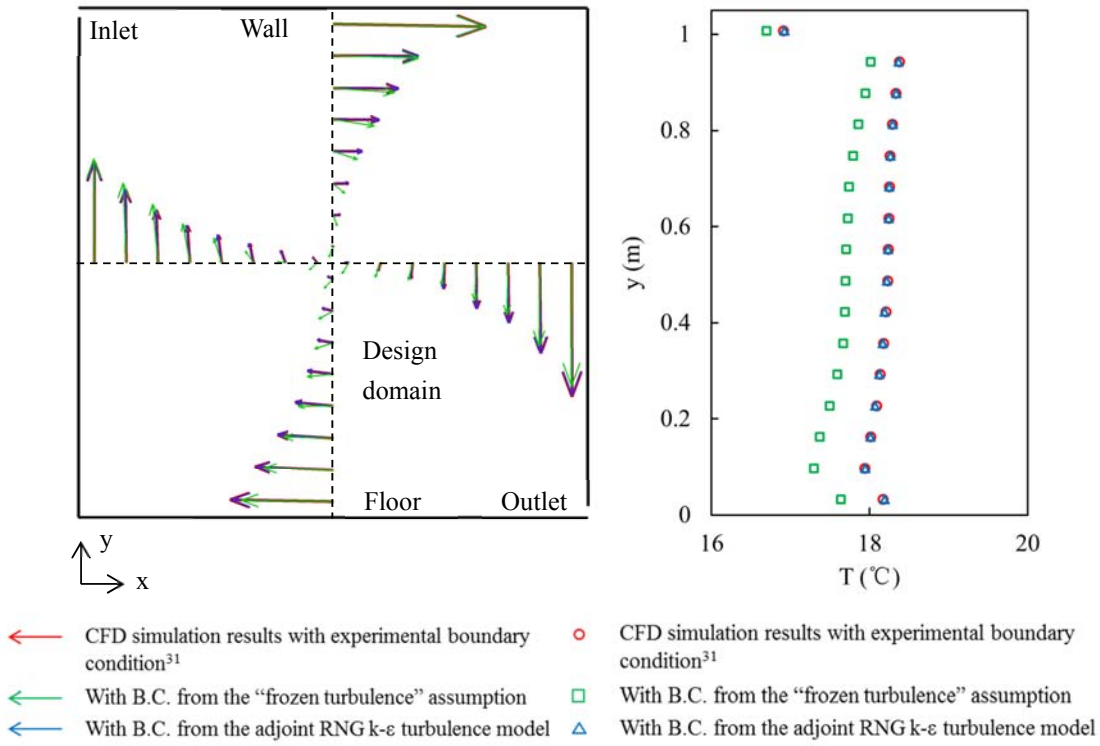

FIGURE 5 Comparison of air velocity vectors in the design domain and temperature profiles at x = 0.5 *l* predicted by the experimental B.C. from Blay et al.[31] and the air supply parameters identified by the adjoint method with the "frozen turbulence" assumption and with the adjoint RNG k-ε turbulence model

3.2 Three-dimensional ventilated office

The second case is a three-dimensional ventilated office, as shown in Figure 6, with experimental data[32]. In the experiment, the office was ventilated by a displacement ventilation system[33] with an air supply velocity of $\mathbf{V}_{inlet}$ = (0.09, 0, 0) m/s and air supply temperature of T_{inlet} = 17 ºC. The air was supplied through a wall diffuser at floor level and exhausted through an outlet at ceiling level. This office was more complicated than the two-dimensional ventilated cavity and closer to reality, although the occupants, computers, cabinets, and lights were all simplified as rectangular boxes. Therefore, it was more practical to use this office for inversely identifying the optimal air supply parameters. Similar to the previous case, we used CFD simulation results along lines 1, 3, 5, 7, and 9 to construct the objective function as expressed by Eqs. (21) and (22). We used a structured grid of hexahedral elements in this geometric model, with 272,513 cells according to our grid-independence tests.

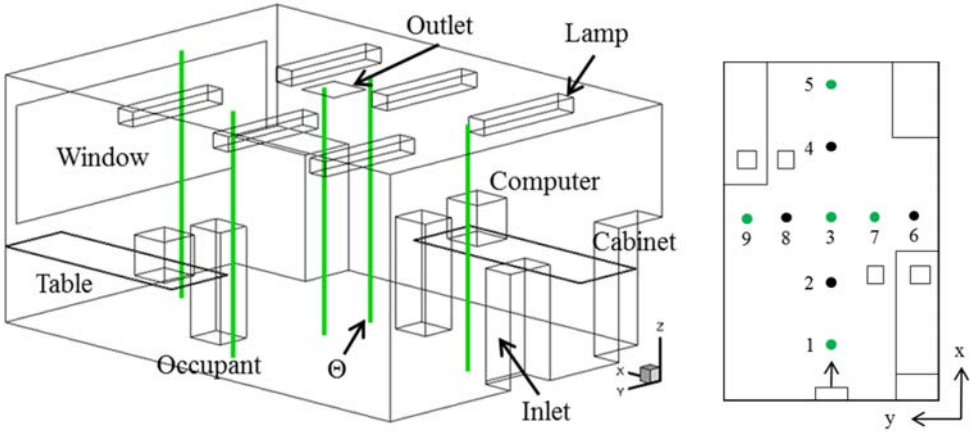

FIGURE 6 Schematic of a two-person office, and the design domain location where the numbers 1 to 9 indicate locations where air velocity and temperature profiles were measured in the experiment[32].

To start the inverse design process, the inlet B.C. were initialized as $\mathbf{V}_{inlet}$ = (0.5, 0, 0) m/s and T_{inlet} = 20ºC. Note that the step sizes for updating $\mathbf{V}_{inlet}$ and T_{inlet} were 0.02 and 100, respectively. Figure 7 shows the variation in the objective function with the design cycle during the inverse design process, with the "frozen turbulence" assumption and with the adjoint RNG k-ε turbulence model. The convergence speed with the "frozen turbulence" assumption was ten times faster than that the adjoint RNG k-ε turbulence model. This occurred because the gradients calculated with the "frozen turbulence" assumption were larger than those calculated with the adjoint RNG k-ε turbulence model in the first two design cycles. However, with the adjoint RNG k-ε turbulence model, one could obtain an objective function close to zero.

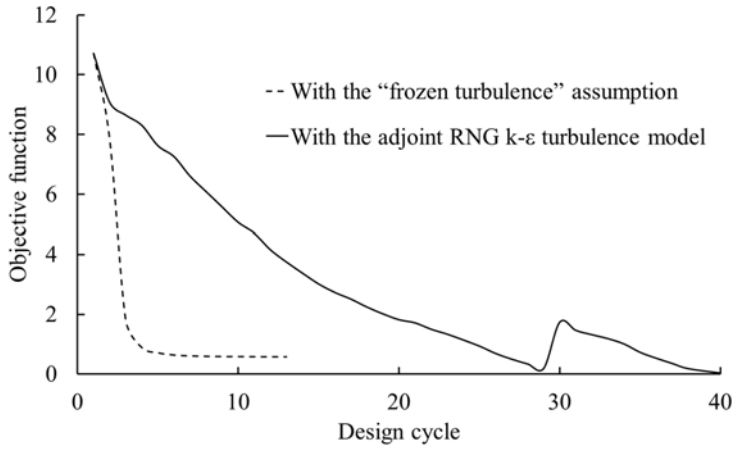

411

412 FIGURE 7 Variation in the objective function with the design cycle for the three-dimensional
413 ventilated office case

414

415 TABLE 2 Design variables identified by two methods compared with experimental B.C.

	$V_{inlet, x}$ (m/s)	$V_{inlet, y}$ (m/s)	$V_{inlet, z}$ (m/s)	T_{inlet} (^{o}C)
With the "frozen turbulence" assumption	0.11	3.0E-4	2.5E-6	17.45
With the adjoint RNG k-ε turbulence model	0.098	6.1E-6	2.1E-6	17.36
Experimental data[32]	0.09	0	0	17.00

416

417 As shown in Table 2, the air supply parameters finally identified by the adjoint RNG k-ε
418 turbulence model were close to the experimental data. We then used these parameters to
419 conduct CFD simulations to determine whether the identified air supply parameters formed
420 the same air distribution as the results with experimental B.C. Figure 8 quantitatively
421 compares the predicted air velocity and air temperature profiles with the experimental profiles
422 at the center of the room (line 3) as an example. The air supply parameters identified by the
423 adjoint RNG k-ε turbulence model were much better than those with the "frozen turbulence"
424 assumption.

425

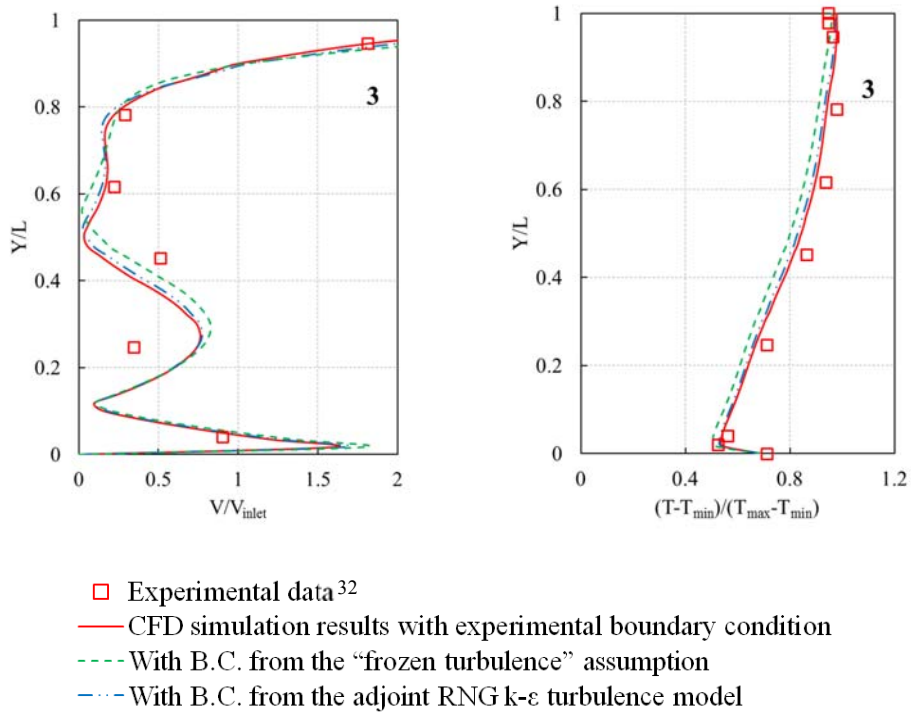

FIGURE 8 Comparison of air velocity and temperature profiles predicted by the experimental B.C. from Yuan et al.[32] and the air supply parameters identified by the adjoint method with the "frozen turbulence" assumption and with the adjoint RNG k-ε turbulence model with the experimental data in the center of the room

3.3 Inverse design of a comfortable indoor environment for the three-dimensional ventilated office

Using the validated adjoint RNG k-ε turbulence model, this investigation next conducted an optimal design of the indoor environment for the two-person office. In the optimal design process, the design domain was the surfaces at a distance of 0.1 m away from the occupants, as shown in Figure 9. We used the predicted mean vote (PMV) [34] to evaluate the thermal comfort level in the domain. The range of PMV values is from -3 to 3, and PMV = 0 signifies a high comfort level. Our design goal was to identify the optimal ξ (air supply velocity $\mathbf{V}_{inlet}$ and air supply temperature T_{inlet}) that would make the average |PMV| in the design domain close or equal to zero. Thus, the objective function can be expressed by

$$J(\xi) = \frac{\int_{\Theta} |\mathrm{PMV}| \, d\Theta}{\int_{\Theta} d\Theta} \tag{23}$$

For a comfortable indoor environment, the air quality must satisfy the design criteria. According to the ASHRAE Handbook[35], the general design criterion used for office buildings is at least 4 air changes per hour, and the corresponding face velocity for this office was 0.086 m/s. Therefore, we added this constraint ($V_{inlet,\,x} \geq 0.086$ m/s) to insure indoor air quality

during the inverse design process.

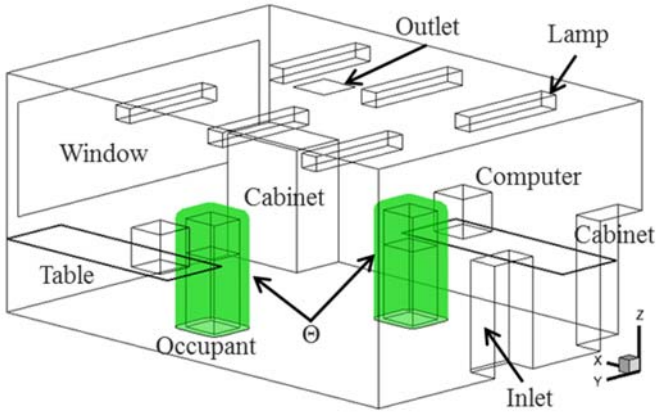

FIGURE 9 Schematic of a two-person office and inverse design domain

Figure 10 depicts the variation in the objective function with the design cycle during the inverse design process. The inverse design process achieved the convergence criterion after 18 design cycles. The final objective function minimized by the adjoint method with the adjoint RNG k-ε turbulence model was 0.122 and did not achieve zero. The reason may be that the objective function was trapped in local optima. The final B.C. identified were $\mathbf{V}_{inlet}$ = (0.184, -5.02E-04, 1.23E-04) m/s and T_{inlet} = 295.16 ºC.

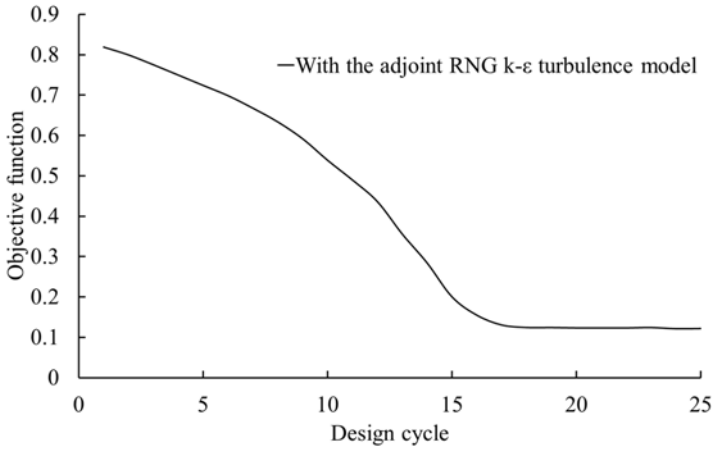

FIGURE 10 Variation in the objective function with the design cycle during the optimal design processes with the adjoint RNG k-ε turbulence model.

Figure 11 depicts the PMV distributions around the occupants inversely designed by the adjoint method with the adjoint RNG k-ε turbulence model. The mean PMV value around the occupant is 0.122 and PMV distributions are all near zero. Hence, the adjoint method with the adjoint RNG k-ε turbulence model has good performance in the optimal design of the indoor environment.

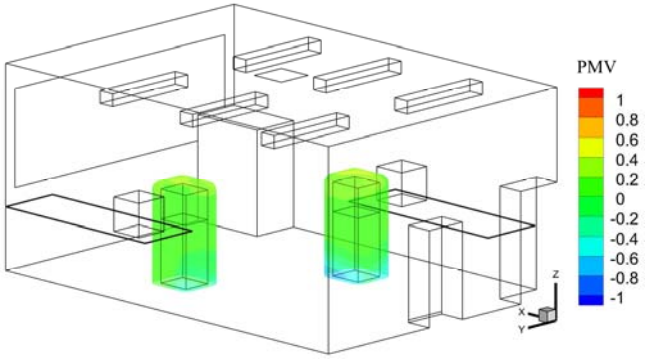

FIGURE 11 PMV distributions around the occupants inversely designed by the adjoint method with the adjoint RNG k-ε turbulence model

4 DISCUSSION

The adjoint RNG k-ε turbulence model improved the optimal design accuracy, but it could not overcome the inherent disadvantages of the adjoint method. The objective function could also become trapped in local optima. If the initial design variables were far away from the optimal values or the step size was not appropriate, the calculation might not lead to the optimal design.

This study used only PMV to evaluate the thermal comfort level and to add a constraint to ensure that the indoor air quality met the standard. With the adjoint method, one could add further design objectives without increasing the computing costs.

The design variables determined in Section 3.3 did not make the objective function equal to zero. This result may imply that the constraints were too restrictive. For example, the design process did not allow changes in the position, size, or shape of the air supply inlets.

For the same case with different objective functions in sections 3.2 and 3.3, the convergence speed is not comparable. This was because the relationship between the objective function and the design variables was not explicit.

This investigation only used the first-order upwind scheme and the central difference scheme to discretize the convection and diffusion terms of the RANS equations closed with the turbulence model and adjoint equations, respectively. While, the influence of different discretization schemes on the inverse design results is not clear at the moment and our future research will conduct an in-depth study and analysis of this issue.

5 CONCLUSIONS

This investigation developed an adjoint RNG k-ε turbulence model for the adjoint method for optimal design of the indoor environment. The following conclusions can be drawn from this study:

- The design process with the adjoint RNG k-ε turbulence model identified design

variables that were more accurate than those identified with the "frozen turbulence" assumption. However, the design variables identified with the "frozen turbulence" assumption were more stable during the inverse design process.

- The adjoint method with the adjoint RNG k-ε turbulence model can be used to design the optimal indoor environment for an office. Design objective could include air velocity distribution, temperature distribution, and the combination of variables calculated by CFD, such as thermal comfort, indoor air quality, etc.
- The design variables must not be overly restrictive. Otherwise, the objective functions may not reach zero, even after numerous design cycles.

ACKNOWLEDGEMENTS

This research was partially supported by the National Key R&D Program of the Ministry of Science and Technology, China, on "Green Buildings and Building Industrialization" through Grant No. 2016YFC0700500 and by the National Natural Science Foundation of China through Grant No. 51478302.

REFERENCES

1. Liu W, Zhang T, Xue Y, et al. State-of-the-art methods for inverse design of an enclosed environment. *Build Environ.* 2015; 91:91-100.

2. Chen Q, Zhai Z, You X, Zhang T. *Inverse Design Methods for Built Environment*. Routledge, Oxford, England; 2017.

3. Chen Q. Ventilation performance prediction for buildings: A method overview and recent applications. *Build Environ.* 2009; 44:848-858.

4. Xue Y, Zhai ZJ, Chen Q. Inverse prediction and optimization of flow control conditions for confined spaces using a CFD-based genetic algorithm. *Build Environ.* 2013; 64:77-84.

5. Wei Y, Zhang TT, Wang S. Prompt design of the air-supply opening size for a commercial airplane based on the proper orthogonal decomposition of flows. *Build Environ.* 2016; 96:131-141.

6. Zhang T, You X. A simulation-based inverse design of preset aircraft cabin environment. *Build Environ.* 2014; 82:20-26.

7. W. Liu, M. Jin, C. Chen, Q. Chen. Optimization of air supply location, size, and parameters in enclosed environments using a computational fluid dynamics-based adjoint method. *J Build Perform Simu.* 2016; 9(2):149-161.

8. Liu W, You R, Zhang J, Chen Q. Development of a fast fluid dynamics-based adjoint method for the inverse design of indoor environments. *J Build Perform Simu.* 2016; 10(3):326-343.

9. Liu W, Chen Q. Optimal air distribution design in enclosed spaces using an adjoint method. *Inverse Probl Sci En*. 2015; 23(5):760-779.

10. Nadarajah S, Jameson A. A comparison of the continuous and discrete adjoint approach to automatic aerodynamic optimization. *In 38th Aerospace Sciences Meeting and Exhibit*. 2000; 667.

11. Liu W, Duan R, Chen C, et al. Inverse design of the thermal environment in an airliner cabin by use of the CFD-based adjoint method. *Energ Buildings*. 2015; 104(2):147-155.

12. Zhao X, Liu W, Lai D, Chen Q. Optimal design of an indoor environment by the

CFD-based adjoint method with area-constrained topology and cluster analysis. *Build Environ.* 2018; 138:171-180.
13. Zhao X, Liu W, Liu S, et al. Inverse design of an indoor environment using a CFD-based adjoint method with the adaptive step size for adjusting the design parameters. *Numer Heat Tr A-Appl*. 2017; 71(7):707-720.
14. Othmer C. A continuous adjoint formulation for the computation of topological and surface sensitivities of ducted flows. *Int J Numer Meth Fl*. 2008; 58(8):861-877.
15. Kim CS, Kim C, Rho OH. Feasibility study of constant eddy-viscosity assumption in gradient-based design optimization. *J Aircraft*. 2003; 40(6):1168-1176.
16. Dwight RP, Brezillon J. Effect of approximations of the discrete adjoint on gradient-based optimization. *AIAA J*. 2006; 44(12):3022-3031.
17. Towara M, Naumann U. A discrete adjoint model for OpenFOAM. *Procedia Computer Science*. 2013; 18:429-438.
18. Papadimitriou DI, Giannakoglou KC. A continuous adjoint method with objective function derivatives based on boundary integrals for inviscid and viscous flows. *Comput Fluids*. 2007; 36 (2):325-341.
19. Zymaris AS, Papadimitriou DI, Giannakoglou KC, Othmer C. Continuous adjoint approach to the spalart-allmaras turbulence model for incompressible flows. *Comput Fluids*. 2009; 38 (8):1528-1538.
20. Zymaris AS, Papadimitriou DI, Giannakoglou KC, Othmer C. Adjoint wall functions: A new concept for use in aerodynamic shape optimization. *J Comput Phys*. 2010; 229 (13):5228-5245.
21. Papoutsis-Kiachagias EM, Zymaris AS, Kavvadias IS, et al. The continuous adjoint approach to the k-ε turbulence model for shape optimization and optimal active control of turbulent flows. *Eng Optimiz*. 2015; 47(3):370-389.
22. Chen Q. Comparison of different k-ε models for indoor air flow computations. *Numer Heat Tr B-Fund*. 1995; 28:353-369.
23. Conceição EZE, Lúcio M. Numerical simulation of the application of solar radiant systems, internal airflow and occupants' presence in the improvement of comfort in winter conditions[J]. *Buildings*, 2016; 6(3): 38.
24. Zhang T, Li P, Zhao Y, Wang S. Various air distribution modes on commercial airplanes-Part 2: Computational fluid dynamics modeling and validation. *HVAC&R Res*. 2013; 19(5):457-470.
25. Zhang Z, Zhang W, Zhai ZJ, Chen QY. Evaluation of various turbulence models in predicting airflow and turbulence in enclosed environments by CFD: Part 2-Comparison with experimental data from literature. *HVAC&R Res*. 2007; 13 (6):871-886.
26. Yakhot V, Orszag S A, Thangam S, et al. Development of turbulence models for shear flows by a double expansion technique [J]. *Phys Fluid Fluid Dynam*, 1992; 4(7): 1510-1520.
27. Ortega BJM, Rheinboldt WC. *Iterative Solution of Nonlinear Equations in Several Variables*. Chap. 8, Academic Press, New York, 1970.
28. Kuzmin D, Mierka O, Turek S. On the implementation of the k-ε turbulence model in incompressible flow solvers based on a finite element discretization. *Int J Comput Math*. 2007; 1(2-4):193-206.
29. OpenFOAM. The Open Source CFD Toolbox. http://www.openfoam.com, 2012.

30. Boussinesq J. *Theorie Analytique de la Chaleur*, Gauthier-Villars; 1903.
31. Blay D, Mergui S, Niculae C. Confined turbulent mixed convection in the presence of a horizontal buoyant wall jet. *Fundamentals of Mixed Convection, ASME HTD*. 1992; 213:65-72.
32. Yuan X, Chen Q, Glicksman LR, et al. Measurements and computations of room airflow with displacement ventilation. *ASHRAE Trans*. 1999; 105:340-352.
33. Zhang TT, Lee K, Chen Q. A simplified approach to describe complex diffusers in displacement ventilation for CFD simulations. *Indoor Air*. 2009; 19(3):255-267.
34. Fanger PO. *Thermal Comfort*. Robert E. Kn'cger Publishing Company, Florida; 1982.
35. ASHRAE. *ASHRAE Handbook - HVAC Applications (SI)*. Atlanta: American Society of Heating, Refrigerating and Air Conditioning Engineers. 2011.